

ANALYSIS OF NONLINEAR RANDOM VIBRATIONS USING ORTHOGONAL DECOMPOSITIONS

Sergio Bellizzi^a and Rubens Sampaio^b

^a*Laboratoire de Mécanique et d'Acoustique, CNRS, 31 chemin Joseph Aiguier, 13402 Marseille, France, bellizzi@lma.cnrs-mrs.fr, <http://www.lma.cnrs-mrs.fr>*

^b*Departamento de Eng. Mecânica, PUC-Rio, Rua Marquês de São Vicente, 225, 22453-900 Rio de Janeiro RJ, rsampaio@puc-rio.br, <http://www.mec.puc-rio.br>*

Keywords: Random vibrations, nonlinear, modal analysis, energy pumping.

Abstract. Orthogonal decompositions provide a powerful tool for random vibrations analysis. The most popular orthogonal decomposition is the Karhunen-Loève Decomposition (KLD). The KLD is a statistical analysis technique for finding the coherent structures in an ensemble of spatially distributed data. The structures (or KL modes) are defined as the eigenvectors of the covariance matrix of the associated random process. Recently, a modified KLD named Smooth Decomposition (SD) has been proposed. The SD can be viewed as a projection of an ensemble of spatially distributed data such that the vector directions of the projection not only keeps the maximum possible variance but also the motions resulting along the vector directions are as smooth as possible in time. The vector directions (or S modes) are defined as the eigenvectors of the generalized eigenproblem defined from the covariance matrix of the random process and the covariance matrix of the associated time derivative random process. It was shown that the SD is an interesting tool to linear random analysis. In this paper, the SD will be used to analyze nonlinear random vibrations. We first focus on the physical interpretation of the S modes. It will be shown that the S modes can be related to the normal modes of the associated linearized system. Finally the ability of KLD and SD to analyze random vibration problem is demonstrated considering an energy pumping phenomena in a linear chain with nonlinear end-attachment.

1 INTRODUCTION

Linear vibration analysis is often based on the normal mode decomposition. When the equations of motion are available, the decomposition can be obtained solving the spectral problem associated to the governing equations. This approach leads to the classical modal analysis where the goal is to describe the structure in terms of its natural characteristics which are the frequency, the damping and the mode shapes. Of course, modal analysis has also been developed from data using temporal and frequency approach (Ewin (1986)).

More generally considering spatio-temporal systems, decomposition methods have been proposed to extract relevant modes from numerical and experiment data. The most popular decomposition is the proper orthogonal decomposition also named Karhunen-Loève Decomposition (KLD) when we refer to random data (see Bellizzi and Sampaio (2006)). The KLD has been used in several domains of engineering science. It can be useful to have a second-moment characterization of a random process in terms of uncorrelated random variables. The basis vectors in this expansion are the eigenvector solutions of the eigenproblem defined from the covariance matrix of the random field under study. The main properties of the KL expansion are the orthogonality of the eigenvectors and the random variables taken as coefficients and the error-minimizing property. Recently, a new multivariable data analysis method called Smooth Decomposition has been proposed (see Chelidze and Zhou (2006) and Bellizzi and Sampaio (2009)). The SD is defined from a maximization problem associated to a scalar time series of measurements subject to a minimization constraint acting on the associated time derivative of the time series. The basis vectors in this expansion are the eigenvector solutions of the generalized eigenproblem defined from the covariance matrix of the random process and the covariance matrix of its time derivative. The SD can be used to extract normal modes and natural frequencies of linear and nonlinear vibration systems and so it is an important tool to analysis data in terms of modal analysis.

In this paper, the KLD and SD will be used and compared to analyze random vibrations of a nonlinear system that presents features of energy capture to passively reduce the vibrations (see Vakakis et al. (2008a)). This phenomenon was principally analyzed in the literature in a deterministic framework. Whereas the main interest is to study of how the properties of the system varies with changes in the parameters, in this first approach the randomness of the system is only due to the forcing term.

Another novelty of this work is the use of the Smooth Decomposition (SD) to study the properties of the system. In the linear case, the normal modes do not depend on the excitation and the behavior of linear system can be completely analyzed through the normal modes. Presently, there is no similar tool in the nonlinear case. The Karhunen-Loève modes depend on the energy levels and they have no easy relation with the frequencies of an associated linear system. So, if one tries to compare properties of a nonlinear system with those of some associated linearization it is not an easy task to use KLD. On the other hand, the SD offers a way to make this comparison since it has a dual interpretation. The modes given by the SD can be ordered through frequency, as normal modes are, and through energy levels, as Karhunen-Loève modes are. This makes the SD a powerful tool to analyze nonlinear systems in a way similar to modal analysis of linear systems or in a way similar to KLD.

The paper is organized as follows. In Section 2, some properties of orthogonal decompositions (KLD and SD) are recalled. In Section 3, the nonlinear system of interest is described and numerical evidences showing that the nonlinear end-attachment is able to absorb vibrations of the linear chain (energy pumping phenomenon) when the excitation is random are

presented. Finally, in Section 4, the energy pumping phenomenon is analyzed using KLD and SD approaches.

2 ORTHOGONAL DECOMPOSITIONS

Let $\{\mathbf{U}(t)\}_t = \{\mathbf{U}(t), t \in \mathbb{R}\}$ be a \mathbb{R}^n -valued random process indexed by \mathbb{R} . We assume that $\{\mathbf{U}(t), t \in \mathbb{R}\}$ is a second-order stationary process that has a time-derivative process $\{\dot{\mathbf{U}}(t), t \in \mathbb{R}\}$ which is also a second-order stationary process. With these assumptions, the covariance matrices of $\{\mathbf{U}(t), t \in \mathbb{R}\}$ and $\{\dot{\mathbf{U}}(t), t \in \mathbb{R}\}$, denoted $\mathbf{R}_U = \mathbb{E}(\mathbf{U}(t)^T \mathbf{U}(t))$ and $\mathbf{R}_{\dot{U}} = \mathbb{E}(\dot{\mathbf{U}}(t)^T \dot{\mathbf{U}}(t))$ respectively, do not depend on time. Without loss of generality, we will also assume that $\{\mathbf{U}(t), t \in \mathbb{R}\}$ is a zero-mean random process and that \mathbf{R}_U and $\mathbf{R}_{\dot{U}}$ are symmetric positive-definite.

2.1 Definition

In vibration problems we usually want to develop a \mathbb{R}^n -valued random process into a series in the separated-variables form

$$\mathbf{U}(t, \theta) = \sum_{k=1}^n a_k(t, \theta) \Phi_k \tag{1}$$

where Φ_k are deterministic \mathbb{R}^n -vectors and $\{a_k(t)\}_t$ are scalar random processes, the θ variable indicates the randomness. If the vectors Φ_k and/or the random processes $\{a_k(t)\}_{t \in \mathcal{D}_T}$ satisfy some orthogonal and optimality properties, the expansion (1) will be called the orthogonal decomposition.

We will consider here two decompositions, the Karhunen-Loève Decomposition (KLD) and the Smooth Decomposition (SD). Each decomposition results from an optimization problem and is built from the covariance matrices \mathbf{R}_U and $\mathbf{R}_{\dot{U}}$.

The optimization problem aims at obtaining the most characteristic constant vectors Φ in the sense that they maximize

$$\max_{\Phi \in \mathbb{R}^n} J(\Phi) \text{ with } J(\Phi) = \begin{cases} J_{KLD}(\Phi) = \frac{\mathbb{E}(\langle \mathbf{U}(t), \Phi \rangle^2)}{\langle \Phi, \Phi \rangle^2} = \frac{\Phi^T \mathbf{R}_U \Phi}{\Phi^T \Phi} & \text{for KLD} \\ J_{SD}(\Phi) = \frac{\mathbb{E}(\langle \dot{\mathbf{U}}(t), \Phi \rangle^2)}{\mathbb{E}(\langle \dot{\mathbf{U}}(t), \dot{\mathbf{U}}(t) \rangle)} = \frac{\Phi^T \mathbf{R}_U \Phi}{\Phi^T \mathbf{R}_{\dot{U}} \Phi} & \text{for SD} \end{cases} \tag{2}$$

Here the inner product \langle, \rangle coincides with the dot product in the Euclidean space \mathbb{R}^n . The objective function J_{SD} used to define the SD differs significantly from that used to define the KLD. The denominator of J_{SD} takes the covariance matrix of the time-derivative process $\{\dot{\mathbf{U}}(t)\}_t$ into account (which justifies the name *smooth* decomposition).

The vectors which solve the optimization problem (2) are solutions of the eigenproblems

$$\begin{aligned} \mathbf{R}_U \Phi_k^{KL} &= \mu_k^{KL} \Phi_k^{KL} & \text{for KLD} \\ \mathbf{R}_U \Phi_k^S &= \mu_k^S \mathbf{R}_{\dot{U}} \Phi_k^S & \text{for SD} \end{aligned} \tag{3}$$

Due to the properties of the matrices \mathbf{R}_U and $\mathbf{R}_{\dot{U}}$, the subsets $\{\Phi_1^{KL}, \Phi_2^{KL}, \dots, \Phi_n^{KL}\}$ and $\{\Phi_1^S, \Phi_2^S, \dots, \Phi_n^S\}$ are basis of \mathbb{R}^n . The KL-basis is orthogonal and \mathbf{R}_U -orthogonal. The S-basis is \mathbf{R}_U -orthogonal and $\mathbf{R}_{\dot{U}}$ -orthogonal. All the eigenvalues are greater than zero.

The orthogonal decompositions of the random process are given by

$$\mathbf{U}(t) = \begin{cases} \sum_{k=1}^n a_k^{KL}(t) \Phi_k^{KL} & \text{for KLD} \\ \sum_{k=1}^n a_k^S(t) \Phi_k^S & \text{for SD} \end{cases} \tag{4}$$

with

$$a_k^{KL}(t) = \Phi_k^{KL^T} \mathbf{U}(t) \text{ and } a_k^S(t) = \frac{\Phi_k^{S^T} \mathbf{R}_U \mathbf{U}(t)}{\Phi_k^{S^T} \mathbf{R}_U \Phi_k^S} = \frac{\Phi_k^{S^T} \mathbf{R}_{\dot{U}} \mathbf{U}(t)}{\Phi_k^{S^T} \mathbf{R}_{\dot{U}} \Phi_k^S}. \quad (5)$$

The following notation will be used: the eigenvalues μ_k^{KL} (respectively μ_k^S) will be called KL Values (KLVs) (respectively S Values (SVs)), the eigenvectors Φ_k^{KL} (respectively Φ_k^S) will be called KL Modes (KLMs) (respectively S Modes (SMs)) and the processes $a_k^{KL}(t)$ (respectively $a_k^S(t)$) will be called the KL Components (KLCs) (respectively S Components (SCs)). Notice that the following ordering, $\mu_1^{KL} \geq \mu_2^{KL} \geq \dots \geq \mu_n^{KL} > 0$, and $\mu_1^S \geq \mu_2^S \geq \dots \geq \mu_n^S > 0$ will be used in the sequel.

2.2 Properties of the orthogonal decomposition

Here we recall the main properties of the two approaches in connection with the modal analysis. A complete description of the properties of the KLD and SD can be found in [Bellizzi and Sampaio \(2006\)](#) and [Bellizzi and Sampaio \(2009\)](#).

2.2.1 Linear case

We assume that \mathbf{R}_U and $\mathbf{R}_{\dot{U}}$ are the covariance matrices of the steady state solution of a discrete linear mechanical system with n degrees of freedom governed by the equation of motion

$$\mathbf{M}\ddot{\mathbf{U}}(t) + \mathbf{C}\dot{\mathbf{U}}(t) + \mathbf{K}\mathbf{U}(t) = \mathbf{F}(t) \quad (6)$$

where \mathbf{M} , \mathbf{C} , and \mathbf{K} are $n \times n$ symmetric matrices and the excitation vector, $\{\mathbf{F}(t)\}_t$, is a zero-mean white-noise random excitation with intensity \mathbf{S}_F (i.e., $\mathbf{R}_F(\tau) = \mathbb{E}(\mathbf{F}(t + \tau)\mathbf{F}^T(t)) = \mathbf{S}_F\delta(\tau)$).

If the damping is proportional and if the modal-excitation terms are uncorrelated then the following results hold:

- the SMs are related to the normal modes by

$$\Phi^S = \Phi^{L-T} \quad (7)$$

where $\Phi^S = [\Phi_1^S \Phi_2^S \dots \Phi_n^S]$ and $\Phi^L = [\Phi_1^L \Phi_2^L \dots \Phi_n^L]$ denotes the modal matrix associated to the undamped free vibrations of (6) (defined from the mass matrix \mathbf{M} and the stiffness matrix \mathbf{K});

- the SVs are related to the natural resonance frequencies by

$$\mu^S = (\Omega^2)^{-1} \quad (8)$$

where $\mu^S = \text{diag}(\mu_k^S)$ and $\Omega^2 = \text{diag}(\omega_k^2)$ with ω_k (where $\omega_1 \leq \omega_2 \leq \dots \leq \omega_n$) denotes the natural resonance frequencies associated to the undamped free vibrations of (6);

- moreover, if the mass matrix is proportional to the identity matrix, then

$$\Phi^{KL} = \Phi^L \quad (9)$$

where $\Phi^{KL} = [\Phi_1^{KL} \Phi_2^{KL} \dots \Phi_n^{KL}]$.

As it will be shown hereafter, the relations (7) and (8) can be used to perform modal analysis from SD.

2.2.2 Nonlinear case

We assume that \mathbf{R}_U and $\mathbf{R}_{\dot{U}}$ are the covariance matrices of the steady state solution of a discrete nonlinear mechanical system with n degrees of freedom governing by the equation of motion

$$\mathbf{M}\ddot{\mathbf{U}}(t) + \mathbf{C}\dot{\mathbf{U}}(t) + \mathbf{K}\mathbf{U}(t) + \mathbf{G}(\mathbf{U}(t), \dot{\mathbf{U}}(t)) = \mathbf{F}(t) \quad (10)$$

where the similar terms have the same meaning as in (6) and \mathbf{G} is a smooth nonlinear function.

Under the assumption that the nonlinear system (10) admits a stationary ergodic probability measure, it can be shown that the stationary covariance matrix of the nonlinear response (10) coincides with to the stationary covariance matrix of the equivalent linear response (as defined in [Kozin \(1988\)](#)). Hence, the KLD (respectively SD) analysis of the stationary response of the non-linear system (10) give the same results that the KLD (respectively SD) analysis of the stationary response of the equivalent linear system except for the KLCs and SCs. Following the results presented in the previous section, the SD can also be viewed as a tool for modal analysis of the nonlinear system, the SMs and SVs of the nonlinear system being interpreted as in reference to the modal characteristics of the linearized system.

3 ANALYSIS OF THE ENERGY PUMPING IN A LINEAR CHAIN WITH NONLINEAR END ATTACHMENT

3.1 Description of the system

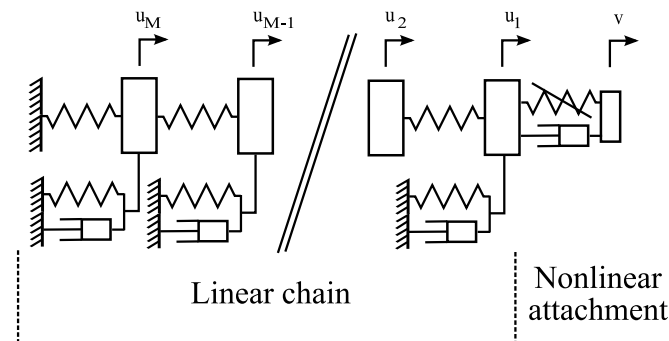


Figure 1: System considered with $(M + 1)$ DOF.

We consider here the system depicted in Fig. 1. This system was studied in [Vakakis et al. \(2003\)](#) considering impulsive excitation. It slightly differs from the one described in [Ma et al. \(2008\)](#) considering the same kind of excitation. The system is composed of a chain of M strongly coupled linear oscillators with a strongly nonlinear end-attachment. The linear chain will be designated as the primary system and the nonlinear end-attachment as the nonlinear absorber. Each mass of the linear chain is connected to the ground by a linear spring and a linear dashpot. The equations of motion are given by

$$m_{NES}\ddot{v} + \lambda_{NES}(\dot{v} - \dot{u}_1) + k_{NES}(v - u_1) + C_{NES}(v - u_1)^3 = 0 \quad (11)$$

$$\ddot{u}_1 + \lambda_0\dot{u}_1 + k_g u_1 - \lambda_{NES}(\dot{v} - \dot{u}_1) - k_{NES}(v - u_1) - C_{NES}(v - u_1)^3 + k_c(u_1 - u_2) = \mathbf{2} \quad (12)$$

$$\ddot{u}_m + \lambda_0\dot{u}_m + k_g u_m + k_c(2u_m - u_{m-1} - u_{m+1}) = 0, \text{ with } m = 1, \dots, M - 1 \quad (13)$$

$$\ddot{u}_M + \lambda_0\dot{u}_M + (k_g + k_c)u_M + k_c(u_M - u_{M-1}) = f(t) \quad (14)$$

where v (respectively u_m) denotes the displacement of the nonlinear end-attachment (respectively the m th mass of the linear chain). All the masses of the primary system are equal and

their common value is 1. All the stiffness coefficients of the linear chain are equal and denoted by k_c . All the stiffness coefficients of the strings connected to the ground are equal and denoted by k_g . It is assumed that the primary system possesses a weak viscous damping (λ_0 is small). The nonlinear end-attachment is constituted of a mass m_{NES} , a linear damper with coefficient λ_{NES} , and a spring including a linear part with coefficient k_{NES} and a cubic part with coefficient C_{NES} . The mass m_{NES} is assumed to be small compared to the total mass of the linear chain and the linear spring is assumed to be small compared to cubic spring.

As described in Vakakis et al. (2003), the nonlinear end-attachment is used here to reduce the vibration of the primary system. In contrast to the classical linear absorber, a nonlinear absorber is capable of reducing the energy of the primary system by targeted energy transfer over a large frequency band. This absorber is called NES (Nonlinear Energy Sink). An overview of this concept can be found in Vakakis et al. (2008a) and Vakakis et al. (2008b). The reason for this energy pumping is the essential stiffness nonlinearity of the nonlinear end-attachment. Since the NES possesses a small linear stiffness component compared to nonlinear part, resonance capture cascades appear between the linear chain and the NES at any mode of the linear chain. This is a series of energy pumping phenomena occurring at different frequencies. This phenomena has been observed and analyzed under deterministic excitations.

We propose here to analyze the targeted energy transfer from the linear chain to the NES when the excitation is random. This kind of excitation differs significantly from the deterministic case considered in Vakakis et al. (2003) or Ma et al. (2008). Here the excitation is only defined from its statistical characteristics and the behavior analysis of the system is based on the stochastic characteristics of the response obtained from the theory of the random vibrations. More precisely, we assume that a random force is applied to the primary system (at the mass number M). This force is of the form

$$f(t) = s_0 W(t) \quad (15)$$

where $\{W(t)\}_t$ is a gaussian white-noise scalar process with intensity one and s_0 denotes the excitation level. We have chosen a white-noise excitation because its Power Spectral Density (PSD) function which describes the relative power contribution at various frequencies is a constant function. In terms of frequency content, a white-noise excitation is similar to an impulsive excitation in the deterministic case. Using a white-noise scalar process permits us to analyze the system without privileging a frequency band.

In the sequel, the stationary responses of the system were investigated and the excitation levels s_0 will be used as the parameter of analysis. The behavior of the stationary responses was studied observing the second order moments and the Power Spectral Density (PSD) functions of the $(M + 1)$ DOF, v, u_1, u_2, \dots, u_M , of the system.

3.2 About the numerical approach

To allow comparison with results on the literature in the deterministic case, the following numerical parameter values were used to simulate the system (11-14): $M = 9$ (that is a 10-DOF system including 9-DOF from the linear chain and 1-DOF from the nonlinear end-attachment), $\lambda_0 = 0.001$, $k_g = 1$, $k_c = 1$, $m_{NES} = 0.05$, $\lambda_{NES} = 0.001$, $k_{NES} = 0.0001$ and $C_{NES} = 1$.

The Monte-Carlo method was used to estimate the stationary responses of the system under random excitation. From a given excitation level, the response time history (displacement and velocity) was obtained from an time history of excitation (15) by solving Eqs. (11-14) over the time interval $[0, t_f]$ numerically using the Newmark method. Zero initial displacement

and velocity were assumed. The time-discretization parameter value was chosen equal to $\Delta t = 0.143$ s (i.e. $f_e = 7$ Hz) and 524286 instants ($t_f = 74942$ s) were simulated. The time histories of $W(t)$ (a gaussian white-noise scalar process with intensity one) were generated using the procedure described in Poirion and Soize (1989).

Assuming ergodicity, the last-half points of the displacement and velocity time histories were used to approximate the second order moments (as the time averages) and the Power Spectral Density functions (as the average of the periodgram considering a window length $NFFT = 4096$).

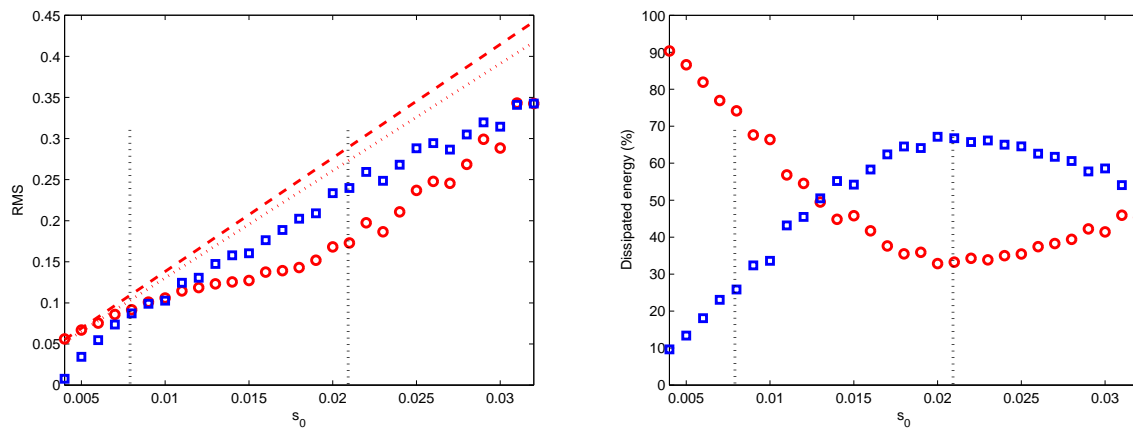


Figure 2: Left: Square root of the trace of the covariance matrix of the vector displacement (u_1, u_2, \dots, u_M) for the system with the NES (red circle markers), for the system without NES (red dashed line) and for the system with only the linear part of the NES (red dotted line), and the RMS values of the displacement v (blue square markers) versus level excitation s_0 . Right: Percentage of energy dissipated by the linear chain (red circle markers) and by the NES (blue square markers) versus level excitation s_0 .

3.3 Passive capacity of vibration reduction

We limit the discussion to some numerical evidences showing that the nonlinear end-attachment is able to absorb vibrations of the linear chain when the excitation is random. The effect of the NES on the linear chain is analyzed comparing the evolution of the second order moments and the Power Spectral Density functions of the chain mass motions (u_1, u_2, \dots, u_M) and the NES mass motion (v) versus the excitation level s_0 . In this numerical study, we have chosen $s_0 \in [0.004, 0.032]$.

In Fig. 2-left, we display the evolution of $RMS_{NES} = \sqrt{\mathbb{E}(v^2(t))}$ (the RMS values of the NES displacement v) and $RMS_{chain} = \sqrt{\mathbb{E}(u_1^2(t)) + \mathbb{E}(u_2^2(t)) + \dots + \mathbb{E}(u_9^2(t))}$ (the square root values of the trace of the covariance matrix of the vector displacement (u_1, u_2, \dots, u_9)) versus s_0 . The evolution of the RMS_{chain} are also reported considering two linear configurations of the system (11-14). The first one corresponds to the system without nonlinear end-attachment (i.e. only the primary system) and the second one corresponds to the system with only the linear part of the end-attachment ($C_{NES} = 0$).

For small s_0 , significant vibrations occur only on the linear chain (see red circle markers in Fig. 2-left) so the behavior of the system is close to the behavior of the two linear configurations (see red dotted and dashed lines in Fig. 2-left). When s_0 increases, the vibrations of the NES mass increase (see blue square markers in Fig. 2-left) and simultaneously the vibrations of the masses of the linear chain are significantly reduced compared to the two linear configurations

(see red circle markers in Fig. 2-left). Particularly interesting is that a zone (defined by $0.008 \leq s_0 \leq 0.021$) appears where RMS_{chain} does not significantly increase with s_0 . This zone will be named "effective" zone. Finally, for large values of s_0 (i.e. $s_0 > 0.021$) the vibrations of the masses of the linear chain again increase linearly.

An important measure to evaluate the performance of NES is the energy dissipated by the nonlinear end-attachment. Based on the model, the energy dissipated by the linear chain and by the NES are respectively given by

$$E_{chain}^d = \lambda_0 \sum_{m=1}^9 \mathbb{E}(\dot{u}_m^2(t)) \text{ and } E_{NES}^d = \lambda_{NES} \mathbb{E}((\dot{v}(t) - \dot{u}_9(t))^2). \quad (16)$$

The percentages of energy dissipated by the linear chain ($E_{chain}^d / (E_{chain}^d + E_{NES}^d)$) and by the NES ($E_{NES}^d / (E_{chain}^d + E_{NES}^d)$) are reported versus the excitation level in Fig. 2-right.

For small s_0 , the energy is mainly dissipated by the linear chain (see red circle markers in Fig. 2-right). When s_0 increases, the percentage of energy dissipated by the linear chain decreases whereas the percentage of energy dissipated by the NES increases. The optimal performance of the NES is obtained for $s_0 \approx 0.021$ where 70% of energy is dissipated by the nonlinear end-attachment (see blue square markers in Fig. 2-right). This value corresponds to the upper bound of the "effective" zone. Finally for large values of s_0 (i.e. $s_0 > 0.021$), the percentage of energy dissipated by the NES decreases whereas the percentage of energy dissipated by the linear chain turns to increase and becomes greater than the percentage of energy dissipated by the NES. The energy pumping phenomena vanishes.

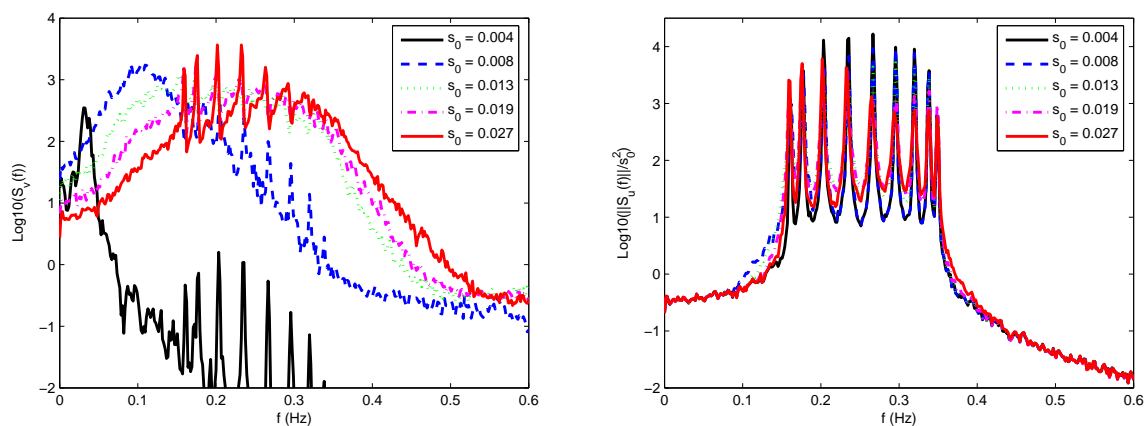


Figure 3: Right: PSD of the displacement of the NES mass versus frequency for five values of s_0 . Left: Frobenius-norm of the PSD matrix of the displacement vector of the M masses of the linear chain for the system with NES normalized by the excitation level for five values of s_0 .

The previous results indicate that the NES (a lightweight nonlinear end-attachment) can modify the dynamic of the linear chain. In reference of the excitation level, three behaviors can be observed. For small values of s_0 (i.e. for small amount of energy transmitted from the excitation source to the linear chain) no coupling appears between the linear chain and the NES. When a specific threshold (in terms of amount of energy transmitted from the excitation source to the linear chain or equivalently in terms of excitation level condition) is exceeded, the vibrations of the NES become large and the vibrations of the linear chain are significantly reduced compared to the linear cases. This is the energy pumping condition, characterized

by a transfer of energy from the primary system to the nonlinear subsystem. This behavior characterizes the "effective" zone. Finally, the energy pumping phenomenon vanishes below a certain level of excitation.

The performance of the NES can also be analyzed in the frequency domain using the PSD function. The PSD describes how the averaged power is distributed as a function of frequency. The peaks on the PSD are related to the frequency components present in the signal which often correspond to the resonance frequencies in vibrations analysis. In Fig. 3-left we display the PSD function of the displacement v of the NES mass and, in Fig. 3-right, the Frobenius-norm of the PSD matrix function of the displacement vector (u_1, u_2, \dots, u_9) characterizing the linear chain. Five values of s_0 will be considered, one ($s_0 = 0.004$) smaller than the threshold, three ($s_0 = 0.008, 0.013$ and 0.019) in the "effective" zone and one ($s_0 = 0.027$) greater than the upper bound of the "effective" zone.

For $s_0 = 0.004$ (black curves in Fig. 3-left and right), the energy on the NES is concentrated around the frequency 0.04 Hz. This frequency is greater than the resonance frequency of the linear part of the NES ($\sqrt{\frac{k_{NES}}{m_{NES}}} \approx 0.0071$ Hz) and little than the first resonance frequency (≈ 0.16 Hz) associated to the linear chain. This peak does not appear on the linear chain (see Fig. 3-right) where only the nine resonance frequencies (0.16, 0.175, 0.21, 0.24, 0.27, 0.3, 0.325, 0.34 and 0.35 Hz) are visible. When s_0 increases from 0.008 to 0.019, the NES PSD shifts from low to high frequencies with spectral broadening showing that the NES acts successively on the increasing seven first modes (from 0.16 Hz to 0.32 Hz) of the linear chain. Simultaneously, when s_0 increases from 0.008 to 0.019, the resonance peaks associated to components of the linear chain are successively "reduced" and slightly shift on the left. Finally, for $s_0 = 0.027$, the NES is still effective.

4 MODAL ANALYSIS BASED ON ORTHOGONAL DECOMPOSITION

The KLD and SD are now used to analyze the dynamics of the system (11-14). The system (11-14) can be written in the form of Eq. (10) where $\mathbf{U} = (v, u_1, u_2, \dots, u_M)^T$. The decomposition parameters were obtained solving the eigenproblems (3) using the covariance matrices $\mathbf{R}_{\mathbf{U}}$ and $\mathbf{R}_{\dot{\mathbf{U}}}$ estimated from the numerical simulations (see Section 3.2). Same data have been used as in Section 3.3.

4.0.1 KLD analysis

In Fig. 4, we show the mode shapes of the four dominant KL modes of the system (11-14) for five different excitation level cases as considered in Fig. 3. We also reported the mode shapes of the normal modes of the underlying linear system (i.e. the system (11-14) with only the linear part of the end-attachment ($C_{NES} = 0$)). In Fig. 5, the percentage of energy captured by each of the four dominant KL modes versus excitation level s_0 as considered in Fig. 2 is displayed.

Considering the percentage of energy captured by the KL modes, we can make the following observations:

- For small s_0 , the energy captured by each of the four dominant modes are small and very close (between 12% and 24%) (see Fig. 5).
- When s_0 increases, the percentage of energy captured by the first mode rapidly increases (see blue curve with cross markers in Fig. 5). This mode becomes dominant in the response. The maximum value of the percentage of captured energy ($\approx 65\%$) is obtained

around $s_0 \approx 0.021$ (the upper bound of the "effective" zone) which also corresponds to the value of the best performance of the NES (see Fig. 2-right).

- For $s_0 = 0.004$, the mode shapes of the first four dominant KL modes coincide with the mode shapes of the first four dominant KL modes of the underlying linear system (i.e. $C_{NES} = 0$) (see blue curves with cross markers in Fig. 4).
- For s_0 greater than the threshold ($s_0 \geq 0.008$), the mode shapes of the first dominant KL mode are nearly identical of the first normal mode of the underlying linear system (i.e. $C_{NES} = 0$) (see Fig. 4-top-left). This mode is spatially localized on the NES. The localization of the mode shape of the dominant KL mode on the NES for large excitation level is an indication of transfer of energy from the linear chain towards the NES.

These observations are similar to that presented in Ma et al. (2008) where impulsive deterministic excitations were used. They confirm that, under random excitation the transfer of energy from the linear chain towards the NES is also due to a localization phenomenon.

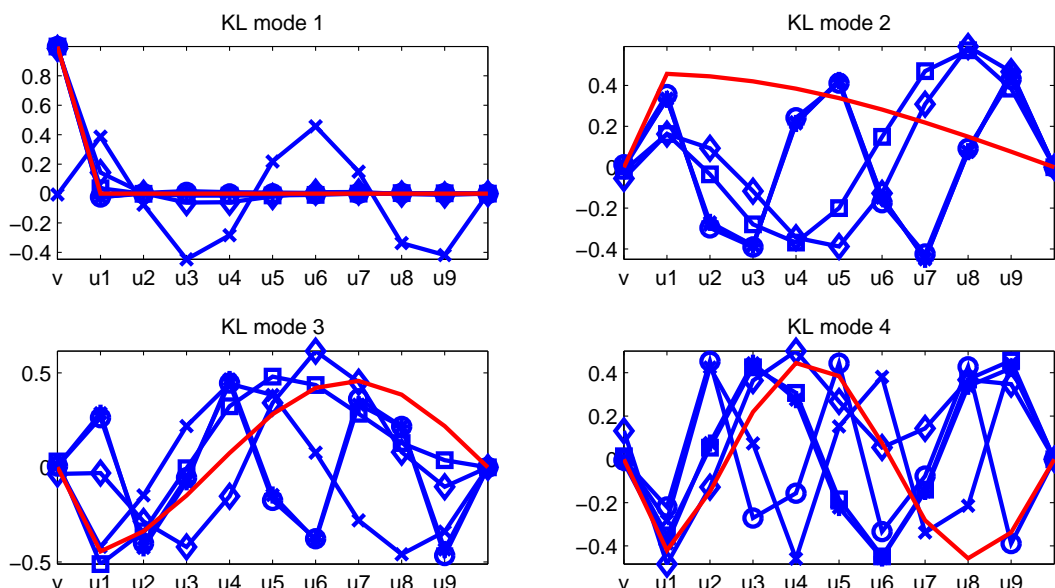


Figure 4: KLD of the system with NES: mode shapes of the four dominant KL modes for $s_0 = 0.004$ (cross markers), $s_0 = 0.008$ (asterisk markers), $s_0 = 0.013$ (circle markers), $s_0 = 0.019$ (square markers) and $s_0 = 0.027$ (diamond marker). The normal modes of the underlying linear system is also depicted (red line).

4.0.2 SD analysis

The SD approach gives access to the S modes but also to the classical modal parameters (the resonance frequencies and the mode shapes) as recalled in Section 2.2. We will focus here on these characteristics.

In Fig. 7 (respectively Fig. 8), the mode shapes of the first (respectively last) four normal modes estimated from the S modes (see Eq. (7)) of the system (11-14) for five different excitation level cases as considered in Fig. 3 are displayed. We also reported the mode shape of the normal modes of the underlying linear system (i.e. $C_{NES} = 0$). In Fig. 6, we display

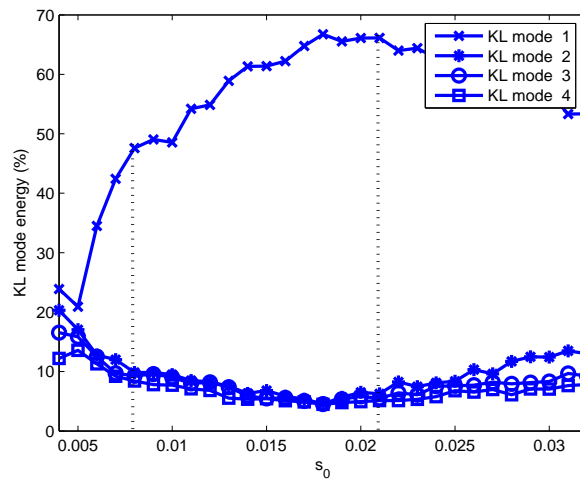


Figure 5: KLD of the system with NES: percentage of energy captured by each of the four dominant KL modes versus level excitation s_0 .

the resonance frequencies estimated from S values (see Eq. (8)) and the percentage of energy captured by the S modes versus excitation level as considered in Fig. 2.

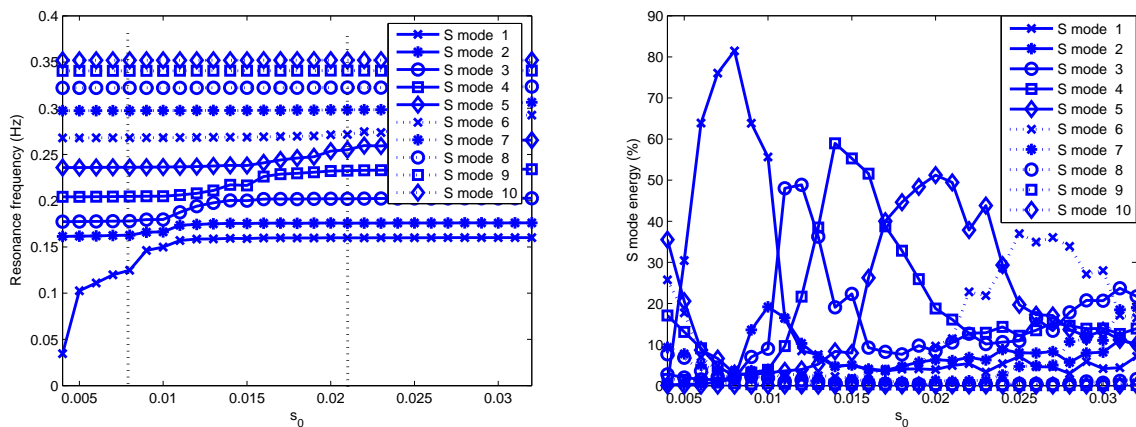


Figure 6: SD of the system with NES: resonance frequencies estimated from SD versus level excitation s_0 (left) and percentage of energy captured by the SKL modes versus excitation level s_0 (right).

Considering the percentage of energy captured by the S modes, we can make the following observations:

- For $s_0 = 0.004$, the ten resonance frequencies estimated from the S values are related to the natural resonance frequencies of the normal modes of the underlying linear system (i.e. $C_{NES} = 0$) (see Fig. 6). The smaller resonance frequency (≈ 0.04 Hz) is greater than the natural frequency of the linear part of the NES, the nine remaining frequencies (0.16, 0.175, 0.21, 0.24, 0.27, 0.3, 0.325, 0.34 and 0.35 Hz) are equal to the natural frequencies of the linear chain. The energy is mainly captured by the S mode number 5, 1, 4, 7 and 8. The mode shapes of the normal modes estimated from the S modes coincide with the mode shapes of the normal modes of the underlying linear system (i.e. $C_{NES} = 0$) (see Figs. 7 and 8).

- For s_0 between 0.04 and 0.08, the first resonance frequency estimated from the S values (see cross markers in (see Fig. 6-left) rapidly increases up to the frequency value 0.16 Hz which corresponds to the natural resonance frequency of the first mode of the linear chain whereas all the nine remaining resonance frequencies estimated from the S values remain constant. For this excitation level band, the energy is captured by the first S mode (see cross markers in Fig. 6-right). The maximum value of the percentage of captured energy ($\approx 82\%$) is obtained for $s_0 \approx 0.008$. For $s_0 = 0.008$, the mode shapes of the first four normal modes estimated from the S modes begin slightly to deviate from the mode shapes of the first four normal modes of the underlying linear system (see Fig. 7) whereas the last four normal modes estimated from the S modes approach remain close to the last four normal modes of the underlying linear system (see Fig. 8).
- Around $s_0 = 0.01$, the second resonance frequency (0.16 Hz) estimated from the S values (i.e. the resonance frequency of the first normal mode of the linear chain) (see blue curve with star markers in Fig. 6-left) begins to increase whereas the first resonance frequency estimated from the S values (see blue curve with cross markers in Fig. 6-left) becomes asymptotic (with respect the excitation level) to 0.16 Hz. For this excitation level, the energy is concentrated on the second S mode (see blue curve with cross markers in Fig. 6-right). At this excitation level, this resonance interaction can be interpreted as a resonance capture.
- Increasing slightly s_0 , the third resonance frequency (0.175 Hz) estimated from the S values (i.e. the resonance frequency of of the second normal mode of the linear chain) (see blue curve with circle markers in Fig. 6-left) begins to increase whereas the second resonance frequency estimated from the S values (i.e. the resonance frequency of the first normal mode of the linear chain) (see blue curve with star markers in Fig. 6-left) becomes asymptotic (with respect the excitation level) to 0.175 Hz. At this level, the energy becomes concentrated on the third S mode. The maximum value of the percentage of captured energy ($\approx 60\%$) is obtained for $s_0 \approx 0.012$ (see blue curve with circle markers in Fig. 6-right). At this excitation level, this resonance interaction can be interpreted as a resonance capture.
- For $s_0 = 0.013$, the mode shapes of the first four normal modes estimated from the S modes differ significantly to the mode shapes of the first four normal modes of the underlying linear system (see Fig. 7) whereas the last four normal modes estimated by the S modes remain close to the last four normal modes of the underlying linear system (see Fig. 8).
- Still increasing the level s_0 , resonance interactions appear involving successively the higher resonance frequencies of the normal mode of the linear chain. This behavior can be interpreted as a resonance captures cascades. This behavior are related to the left shift of the resonant peak observed on the PSD of (u_1, u_2, \dots, u_M) (see Fig. 3-right).

Compared to the KLD analysis, more informations have been deduced from the SD analysis. In particular, the resonance capture phenomenon as well as the resonance captures cascades phenomenon have been revealed. These observations are very similar to that presented in [Vakakis et al. \(2003\)](#) where impulsive excitations were used.

As presented in [Bellizzi and Sampaio \(2010\)](#), a complementary analysis can be derived from the SD approach ordering the S modes with respect to the energy captured by each S mode

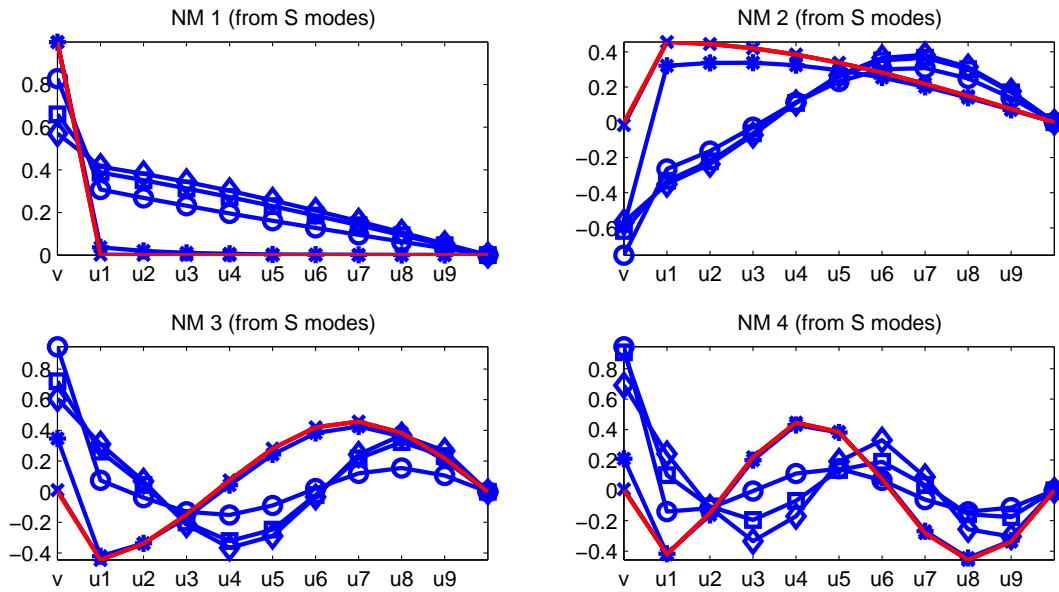


Figure 7: SD of the system with NES: the first four normal modes estimated from the S modes for $s_0 = 0.004$ (cross markers), $s_0 = 0.008$ (asterisk markers), $s_0 = 0.013$ (circle markers), $s_0 = 0.019$ (square markers) and $s_0 = 0.027$ (diamond marker). The normal modes of the underlying linear system is also depicted (red line).

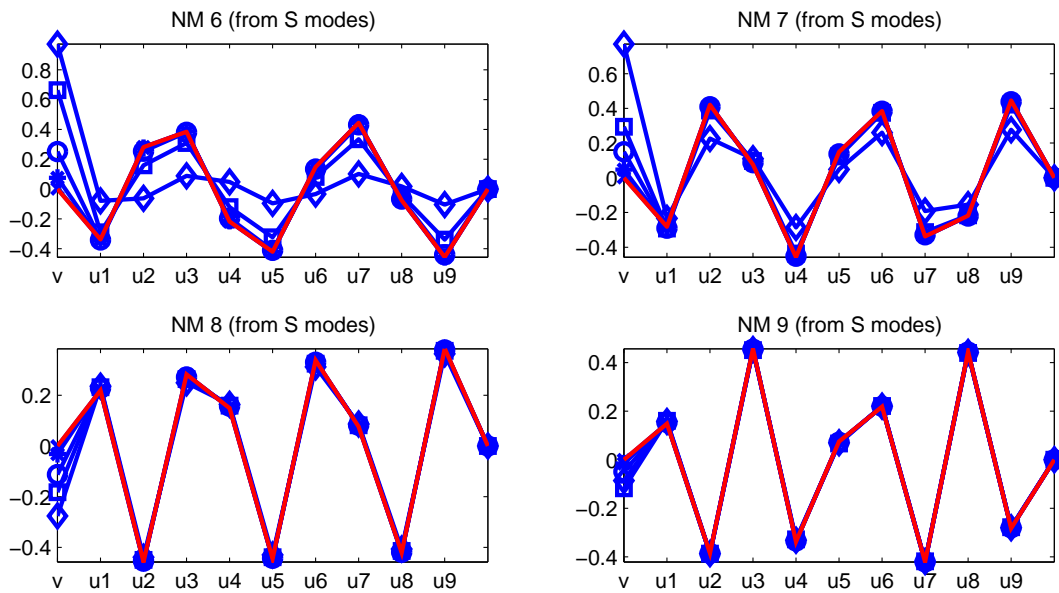


Figure 8: SD of the system with NES: the last four normal modes estimated from the S modes for $s_0 = 0.004$ (cross markers), $s_0 = 0.008$ (asterisk markers), $s_0 = 0.013$ (circle markers), $s_0 = 0.019$ (square markers) and $s_0 = 0.027$ (diamond marker). The normal modes of the underlying linear system is also depicted (red line).

(i.e. the energy of the S components) starting from the highest energy component to the lowest one. In Fig. 10, the mode shapes of the first four normal modes estimated from the S modes ordering with respect the energy of the S components are displayed for five different excitation level cases as considered in Fig. 3. We also reported the mode shape of the normal modes of the underlying linear system (i.e. $C_{NES} = 0$). In Fig. 9, we display the resonance frequencies

estimated from S values and the percentage of energy captured by the S modes versus excitation level versus s_0 as considered in Fig. 2.

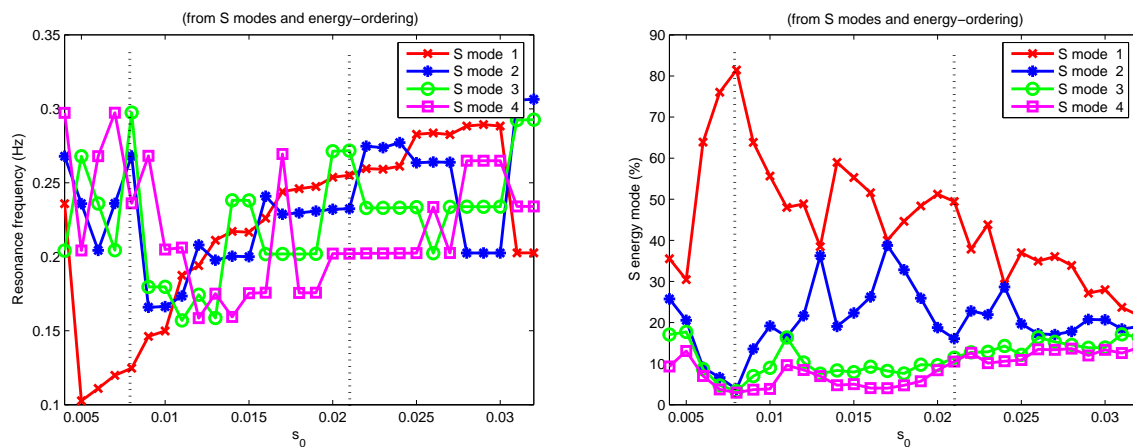


Figure 9: SD of the system with NES: resonance frequencies of the first four normal modes estimated from the S modes ordering with respect to the modal energy versus excitation level s_0 (left) and percentage of energy captured by the four dominant S modes versus excitation level s_0 (right).

From the Figs. 9 and 10, we can make the following observations:

- For small s_0 ($s_0 \leq 0.08$), the resonance frequency of the first energetic dominant S mode coincides with the smaller resonance frequencies (associated to the nonlinear end-attachment) (see Fig. 9-left). This resonance frequency increase with s_0 . The resonance frequencies of the next three energetic dominant S mode take values in the sets $\{0.21, 0.24, 0.27, 0.3\}$ of four natural resonances frequencies of the underlying linear system (i.e. $C_{NES} = 0$). The percentage of energy captured by the first S mode rapidly increases (see cross markers in Fig. 9-right). This mode becomes more dominant in the response. The maximum value of the percentage of captured energy (82%) is obtained for $s_0 = 0.008$.
- When s_0 increases ($s_0 \geq 0.08$), the resonance frequency of the first energetic dominant mode increases defining a branch (see red curve in Fig. 9-left) which crosses all the zones where resonance interactions have been observed in Fig. 6. Moreover, the resonance frequencies (see blue, green and magenta curves in Fig. 9-left) of the next three energetic dominant modes rapidly decrease around 0.18 Hz and next increase fluctuating around the red branch. Here the first two modes becomes more dominant in the response (see cross and star markers in Fig. 9-right).
- For $s_0 = 0.004$, the mode shapes of the first four energetic dominant S modes coincide with the mode shapes of the first four dominant KL modes of the underlying linear system (i.e. $C_{NES} = 0$) (see blue curves with cross markers in Fig. 10).
- For $s_0 \geq 0.008$, the mode shapes of the first energetic dominant normal modes are nearly identical of the first normal mode of the underlying linear system (i.e. $C_{NES} = 0$) (see red curve and curves with square, circle and diamond markers in Fig. 10). This mode is spatially localized on the NES. The localization of the mode shape of the energetic dominant S mode on the NES for large excitation level is an indication of transfer of energy from the linear chain towards the NES.

These observations are very similar to that obtained with the KL analysis. They confirm the importance of the ordering of the S modes. Two ordering can be used for S modes, one, the μ -ordering as presented in Eqs. (7) and (8), is correlated to the classical ordering of the resonance frequencies, the other, the energy-ordering, is correlated with the ordering used for KL modes.

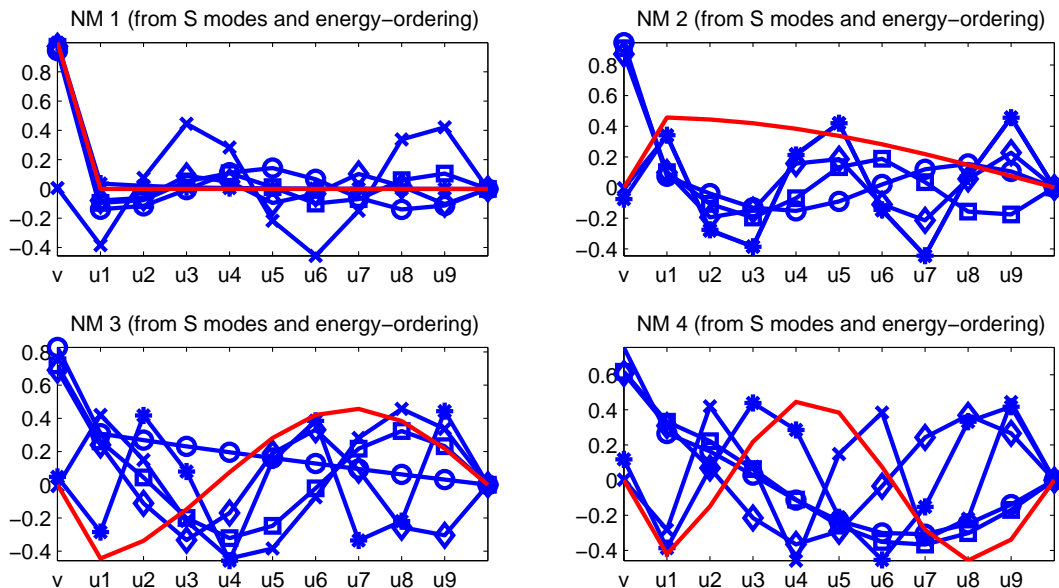


Figure 10: SD of the system with NES: mode shapes of the first four normal modes estimated from the S modes ordering with respect to the modal energy for $s_0 = 0.004$ (cross markers), $s_0 = 0.008$ (asterisk markers), $s_0 = 0.013$ (circle markers), $s_0 = 0.019$ (square markers) and $s_0 = 0.027$ (diamond markers). The normal modes of the underlying linear system is also depicted (red line).

5 CONCLUSIONS

In this paper, a random nonlinear system that presents energy pumping phenomenon is analyzed using KLD and SD. The system presents features very similar to the ones observed in the deterministic case when the system is impulsively forced although the tools of analysis are completely different. The energy pumping occurs for some excitation level, it is due to a localization phenomenon and resonance captures with any mode of the system (in resonance captures cascades). The results confirm the efficiency of the SD. The smooth modes represent well how the energy is distributed in the system and clearly point out the localization phenomenon (as KLD does) and the resonance captures cascades (KLD does not). Contrary to KLD, it is also remarkable how the distribution of energy is related to the frequencies associated with the SD.

ACKNOWLEDGMENTS

The authors gratefully acknowledge the financial support of CAPES and COFECUB (Grant number Ph 672/10).

REFERENCES

Bellizzi S. and Sampaio R. POMs analysis of randomly vibrating systems obtained from Karhunen-Loève expansion. *Journal of Sound and Vibration*, 297:774–793, 2006.

- Bellizzi S. and Sampaio R. Smooth Karhunen-Loève decomposition to analyze randomly vibrating systems. *Journal of Sound and Vibration*, 325:491–498, 2009.
- Bellizzi S. and Sampaio R. Model reduction based on Karhunen-L'ève decomposition and smooth decomposition for random mechanical systems. In *Proceeding of International Conference on Noise and Vibration Engineering (ISMA2010), Leuven : Belgique (2010)*. 2010.
- Chelidze D. and Zhou W. Smooth orthogonal decomposition-based vibration mode identification. *Journal of Sound and Vibration*, 292:461–473, 2006.
- Ewin D. *Modal Testing: Theory and Practice*. Wiley, 1986.
- Kozin F. The method of statistical linearization for nonlinear stochastic vibrations. In *Nonlinear Stochastic Dynamic Engineering Systems (IUTAM Symposium Innsbruck/Austria 1987)*, Spinger, Berlin. 1988.
- Ma X., Vakakis A., and Bergman L. Karhunen-Loève analysis and order reduction of the transient dynamics of linear coupled oscillators with strongly nonlinear attachments. *Journal of Sound and Vibration*, 309:569–587, 2008.
- Poirion F. and Soize C. Simulation numérique des champs stochastiques gaussiens homogènes et non homogènes. *La recherche Aérospatiale*, 1:41–61, 1989.
- Vakakis A., Gendelman O., Bergman L., McFarland D., Kerschen G., and Lee Y. *Nonlinear Targeted Energy Transfer in Mechanical and Structural Systems I*. Springer, 2008a.
- Vakakis A., Gendelman O., Bergman L., McFarland D., Kerschen G., and Lee Y. *Nonlinear Targeted Energy Transfer in Mechanical and Structural Systems II*. Springer, 2008b.
- Vakakis A., L.I. Manevitch L., O. Gendelman O., and Bergmand L. Dynamics of linear discrete systems connected to local essentially non-linear attachments. *Journal of Sound and Vibration*, 264, 2003.